An Analysis of the Potential for Extreme Temperature Change Based on Observations and Model Simulations

Barry H. Lynn

Center for Climate Systems Research, Columbia University, and NASA Goddard Institute for Space Studies, New York, New York

Richard Healy

Woods Hole Oceanographic Institution, Woods Hole, Massachusetts

Leonard M. Druyan

Center for Climate Systems Research, Columbia University, and NASA Goddard Institute for Space Studies, New York, New York

(Manuscript received 29 June 2005, in final form 25 September 2006)

ABSTRACT

The study analyzes observational climate data for June–August 1977–2004 and simulations of current and future climate scenarios from a nested GCM/regional climate model system to assess the potential for extreme temperature change over the eastern United States. Observational evidence indicates that anomalously warm summers in the eastern United States coincide with anomalously cool eastern Pacific sea surface temperatures, conditions that are conducive to geopotential ridging over the east, less frequent precipitation, and lower accumulated rainfall. The study also found that days following nighttime rain are warmer on average than daytime rain events, emphasizing the importance of the timing of precipitation on the radiation balance. Precipitation frequency and eastern Pacific sea surface temperature anomalies together account for 57% of the 28-yr variance in maximum surface temperature anomalies. Simulation results show the sensitivity of maximum surface air temperature to the moist convection parameterization that is employed, since different schemes produce different diurnal cycles and frequencies of precipitation. The study suggests that, in order to accurately project scenarios of extreme temperature change, models need to realistically simulate changes in the surface energy balance caused by the interannual variation of these precipitation characteristics. The mesoscale model that was realistic in this respect predicted much warmer mean and maximum surface air temperatures for five future summers than the parallel GCM driving simulation.

1. Introduction

The potential for extreme climate change has gained currency in contemporary discussions about the environment (e.g., Meehl et al. 2000; Diffenbaugh et al. 2005). A "run" of extreme maximum temperatures is usually correlated with the mean temperature regime (e.g., Mearns et al. 1984). However, while results of general circulation model (GCM) experiments project large-scale aspects of global climate change, GCMs do not typically resolve details of synoptic-scale patterns and associated precipitation that lead to more extreme regional events. Alternatively, GCMs have been used as the "global driver" for regional-scale mesoscale models to simulate regional climate (e.g., Bates et al. 1993; Giorgi et al. 1993; Walsh and McGregor 1995; Nobre et al. 2001; Leung et al. 2003a,b), and to project regional climate change decades into the future (Bell et al. 2004; Han and Roads 2004; Leung et al. 2004; Liang et al. 2004).

A widely used mesoscale model for regional downscaling is the fifth-generation Pennsylvania State University–National Center for Atmospheric Research (NCAR) Mesoscale Model (MM5; Dudhia 1993; Grell et al. 1994). Lynn et al. (2004) studied an MM5-simulated climate change scenario for individual sum-

Corresponding author address: Leonard M. Druyan, Center for Climate Systems Research, Columbia University, and NASA Goddard Institute for Space Studies, 2880 Broadway, New York, NY 10025.
E-mail: LD12@columbia.edu

DOI: 10.1175/JCLI4219.1

© 2007 American Meteorological Society

mers in "time slice" mode. The simulations were initialized with the soil and atmospheric conditions of the atmosphere–ocean GCM (AOGCM) of the Goddard Institute for Space Studies (GISS; Russell et al. 1995, 2000; Lucarini and Russell 2002) and forced with lateral boundary conditions also from the GISS AOGCM. Applications of their results included evaluations of climate change impacts on air quality (Hogrefe et al. 2004), and an assessment of the effect of heat stress on future mortality (Knowlton et al. 2004).

Lynn et al. (2004) found that it was possible to examine the effect of the timing of precipitation on simulated temperatures by using two different cumulus parameterizations in the MM5: commonly referred to as the "Betts–Miller" and the "Grell" schemes (both discussed below). They found that the Betts–Miller scheme favors the development of moist convection when advective processes lead to large-scale destabilization of the atmosphere. In nature, this often occurs in the U.S. plain states at night or early morning (Hu and Feng 2002). However, nocturnal maxima were also widely simulated with Betts–Miller in the southeastern United States as well, where boundary layer processes should favor the triggering of afternoon moist convection (Trenberth et al. 2003). MM5 simulations with the Grell scheme, on the other hand, simulated a preponderance of early afternoon precipitation in the southeast while favoring nighttime precipitation in the Plains states (Lynn et al. 2004).

Lynn et al. (2004) concluded that, in climate change experiments, the mean decadal temperature (T) was quite sensitive to the modeled timing of precipitation, as simulated using either Betts–Miller or Grell. A preponderance of nighttime precipitation obtained with the Betts–Miller scheme maximized T through a shortwave/longwave radiation feedback. The timing of precipitation in Grell, on the other hand, limited the potential increase in the maximum T in the changing climate: there was less solar heating in the afternoon, and more longwave radiation was lost to space at night.

Recognizing that climate extremes over shorter time scales such as months or summer seasons are also of great interest, this paper investigates the relationship between the interannual variability of observed and simulated summer precipitation and maximum T in the eastern United States. We also examine potential relationships between T and observed sea level pressure, surface, winds, geopotential height, and sea surface temperatures to put these results in a broader context. Finally, we evaluate AOGCM/MM5 system projections of future climate trends in the context of the empirical analysis to assess their implications for extreme temperature change.

2. Data and methods

The initial analysis is based on surface station observations of hourly temperatures, sea level pressure, and precipitation, obtained from the Data Support Section (DSS) at the National Center for Atmospheric Research (NCAR) for the available 28 yr from 1977 to 2004. The domain for the analysis extends from 30° (the southern border of the United States) to 47°N (near the northern border), and from 95° to 71°W (the Kansas–Nebraska border to the Atlantic Ocean coast).

Regression analysis investigated the relationships between variables. For 28 pairs of data (28 seasons), the confidence levels for rejecting the null hypothesis correspond to the following correlation coefficients: $r \geq 0.37$, $P = 95\%$; $r \geq 0.44$, $P = 97\%$; and $r \geq 0.48$, $P = 99\%$.

The sensitivity of daily maximum T to sea surface temperatures (SST) was investigated. A number of articles have been published examining the relationship between SST and regional climate, using indices such as the "North Atlantic Oscillation," etc. (e.g., Kushnir and Lau 1992; Kushnir 1994; Bunkers et al. 1996; Lau 1997; Ting and Wang 1997; Ye 2001; Straus and Molteni 2004). Many of these, however, did not deal with the effect of changes in SST on summer temperatures in the eastern United States. For example, Ting and Wang (1997) examined the effect of Pacific SST on the northern Plains climate. Here we consider spatial averages of National Centers for Environmental Prediction (NCEP) reanalysis of June–August (concurrent) SST in the eastern Pacific and western Atlantic, computed over the ocean areas: 15°–60°N, 105°–145°W in the Pacific and 15°–60°N, 50°–80°W, in the Atlantic. Atlantic and Pacific June–August (JJA) SST anomalies (SSTAs) relative to the 28-yr mean were normalized by dividing by the standard deviation of their respective 1977–2004 time series. As part of the evaluation of a possible link between SST and atmospheric variables in the eastern United States, we also examined the interannual variability of regional mean JJA 500-mb geopotential heights obtained from NCEP reanalysis data. The domain for these regional means is the same as for surface air temperature (30°–47°N, 71°–95°W).

GISS AOGCM simulations, including modeled SST, for JJA 1993–97, with annually increasing concentrations of greenhouse gases and aerosols, were used to force MM5 simulations of the "current" climate. For the climate change experiments, the MM5 was driven by the GISS AOGCM simulations of the Intergovernmental Panel on Climate Change (IPCC) A2 climate change scenario for individual (time slice) summers in the 2080s. The modeling system was initialized at the

beginning of each May, to allow enough spinup time to develop synoptic and mesoscale atmospheric "signals." The simulations used the GISS AOGCM soil temperature and moisture interpolated to the MM5 grid as part of the initial (1 May) conditions.

Russell et al. (1995) described the AOGCM structure. It was run on a 4° × 5° horizontal grid with nine vertical layers in σ, or "terrain-following" coordinates, and a maximum of 13 vertical ocean layers. The calculation of a linear gradient allows subgrid-scale effects to be included in the physics. For example, atmospheric convection is done on quarter-grid boxes, by assessing the moist static energy profile (a function of temperature and moisture, each of which is known on quarter-grid resolution). Hence the resolution for specific physics subroutines occurs on a finer scale than indicated by the gridbox resolution alone. Cloud liquid water is not monitored. The atmospheric mass and momentum equations are solved on a modified version of the "C grid" scheme. In addition to calculating the mean (potential) temperature and moisture in each grid box, the model also calculates the gradient of these fields as prognostic variables by using a linear upstream scheme for heat and moisture advection, with subgrid-scale linear gradients in three dimensions. The radiation scheme is the same as in the GISS GCM Model II (Hansen et al. 1983), except that the optical depths for cloud cover were altered so as to provide a better agreement with observations of solar radiation at the surface. The ocean model is also run at 4° × 5° resolution, but the linear upstream scheme is used for potential enthalpy and salt advection. Potential enthalpy is the prognostic variable rather than potential temperature since it accounts for variations in specific heat capacity (a function of temperature and salinity). The physics incorporated in the ocean includes convection, vertical diffusion, and bottom friction.

Simulations with the MM5 used double-nested 108-/36-km horizontal grids (Fig. 1) and 35 vertical sigma coordinate levels. Simulated maximum temperatures were averaged over the region 30°–47°N, 71°–95°W, which excludes the buffer zone between the 108- and 36-km domains. The 108-km domain was composed of 46 × 56 grid elements, while the 36-km domain had 64 × 79 grid elements (where the larger number refers to the east–west dimension). The 108-km grid was one-way nested within the GISS AOGCM, while the 36-km domain was two-way nested within the 108-km MM5 grid. The MM5 incorporated the boundary layer model from the Medium-Range Forecast Model (MRF); the Betts–Miller, Grell or Kain–Fritsch cumulus parameterizations; and the Rapid Radiative Transfer Model (RRTM), which calculates shortwave and longwave radiation transfer through the atmosphere.

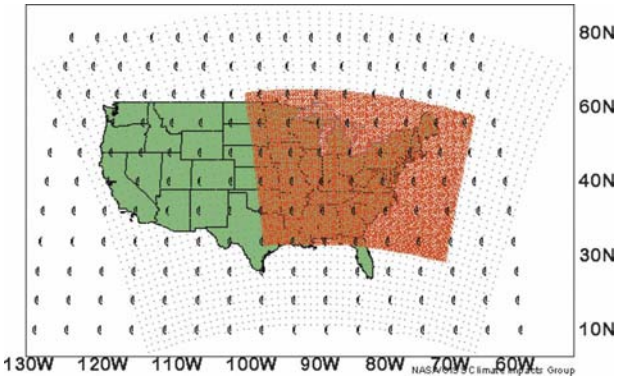

Fig. 1. Domains for MM5 simulations. The red area represents the inner domain for nested simulations on the 36-km grid, black dots indicate data points on the 108-km grid, and heavy marks are the centers of AOGCM grid elements.

MM5 results, discussed below, are sensitive to the choice of cumulus parameterization. Accordingly, these schemes are explained in greater detail. The Betts–Miller is a "relaxation" scheme (Betts 1986; Betts and Miller 1986; Janjic 1994) that does not have explicit triggering of moist convection. In contrast, the version of the Grell scheme used here did include explicit triggering of moist convection, although the original version did not (Grell et al. 1991; Grell 1993). Because it relaxes the whole temperature and moisture profile in one step, in contrast to the Grell assumption of "quasi-equilibrium," the typical Betts–Miller convective event generates more rainfall than a Grell scheme event. The Kain–Fritsch scheme (Kain and Fritsch 1993) assigns a temperature perturbation to a potential cloud parcel based on the grid-scale vertical velocity. It then tests 100-mb layers of atmosphere, beginning with the lowest layer, to determine whether the cloud parcels with their respective temperature perturbations would be buoyant. This procedure is repeated up to the 700- to 600-mb layer. The use of a triggering function in this scheme allows convective available potential energy (CAPE) to build before triggering, but subsequently releases CAPE even when the sounding itself is only conditionally unstable. If the parcel is able to reach its level of free convection, then the impact of convection on temperature and moisture profiles is proportional to the potential buoyant energy, forcing this energy to be removed by the end of the convective period (30 min–1 h).

There are several differences between the three convection schemes. Kain–Fritsch depends on a temperature perturbation proportional to the grid-scale vertical velocity and the CAPE itself, rather than the rate of

change of destabilization due to advection (and in our modified Grell scheme, radiative and boundary layer forcing). Second, Grell "decides" whether or not to be activated every time step, while Kain–Fritsch remains activated until the complete removal of the potential buoyant energy. Hence, once activated, Kain–Fritsch may lead to longer lasting clouds and moist convection than Grell. Moreover, Kain–Fritsch detrains water from the convective scheme directly to the grid-resolved variables.

The land surface model (Chen and Dudhia 2001a,b) was used here to calculate the bottom boundary condition of the model, using interactive soil and vegetative layers, and calculations of a surface energy balance for the combined ground vegetation surface. The MM5 calculates 2-m temperatures from similarity relationships based on skin (radiometric) temperature and the temperature at the first model layer, in this case located at 35 m.

In the time slice approach, the nested mesoscale model simulations are made only for the seasons of interest, saving considerable computer time that would be required for continuous simulations, for example, from June 1993 to August 1997 and from 1997 to 2087. However, continuous MM5 simulations would probably yield somewhat different answers, since the initial conditions on 1 June would include benefits of the long integration at high horizontal resolution and the benefits of soil moisture distributions that are in better equilibrium with the MM5 atmosphere. Since the MM5 used here does not have a dynamic ocean, SST supplied from the AOGCM for oceanic parts of the lower boundary force the MM5 atmosphere, but are not interactive with it. This allows energy to be created or to disappear at the ocean surface, as in any prescribed SST experiment.

3. Results

a. Observational analysis

We consider the interannual variability of station-observed JJA mean maximum daily temperature anomalies (hereafter, ΔT_y, computed for each year relative to the 28-yr mean maximum temperature). Note that all calculations refer to the regional means of each quantity, taking into account observations from all observing stations. We examined the relationship between ΔT_y and variables that are typically used to characterize the synoptic pattern. Interannual variations of ΔT_y were not correlated with the interannual variations of surface pressure anomalies or meridional or zonal wind anomalies. Correlations between ΔT_y and 500-mb NCEP reanalysis geopotential heights are discussed below.

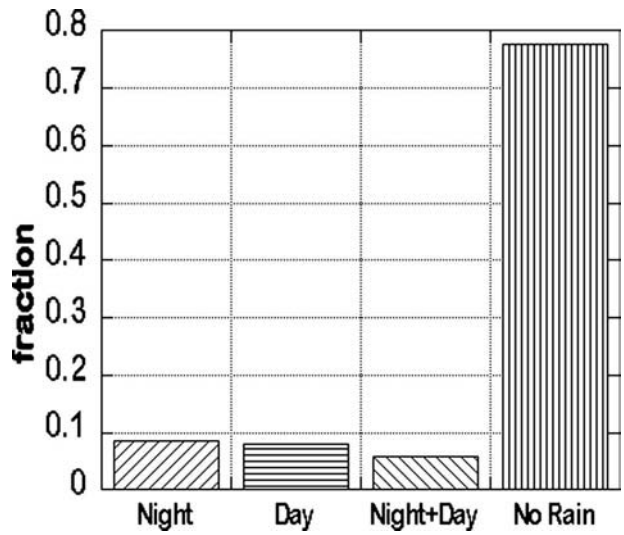

FIG. 2. The fractions of all observed events in the four categories: nighttime (1500–0400 LST) rain, daytime (0500–1400 LST) rain, nighttime and daytime rain, and no rain, during JJA 1977–2004.

The relationship between ΔT_y versus precipitation characteristics was investigated. To this end, the diurnal cycle of rainfall at all stations was analyzed. Figure 2 summarizes the characteristics of the diurnal cycle by indicating the relative percentages of station observations during 1977–2004 in each of four categories, based on when precipitation was recorded within the diurnal cycle: day only [0500–1400 local standard time (LST)], night only (1500–0400 LST), day and night, and no rain during the 24-h period. This partition between "nighttime" and "daytime" rainfall was designed to relate more to the diurnal cycle of the near-surface radiation budget than to darkness versus daylight. Specifically, the designation "daytime rainfall" refers to precipitation during the hours when there is usually a net downward radiation flux responsible for increasing the surface temperature as it climbs to the diurnal maximum. Some 78% of summer dates were completely rain-free, while rain confined only to the overnight hours occurred slightly more frequently than rain confined to the daytime, or dates with rain during both night and day. These differences in timing are next shown to influence maximum surface air temperatures.

Figure 3 shows that the 28-yr mean ΔT_y was positive for only the category of dates with no rain. Note, however, that the 28-yr mean ΔT_y for the category with nighttime rain was less negative than for dates in the category of daytime rain. Days without rain were warmer than days with rain most probably because of

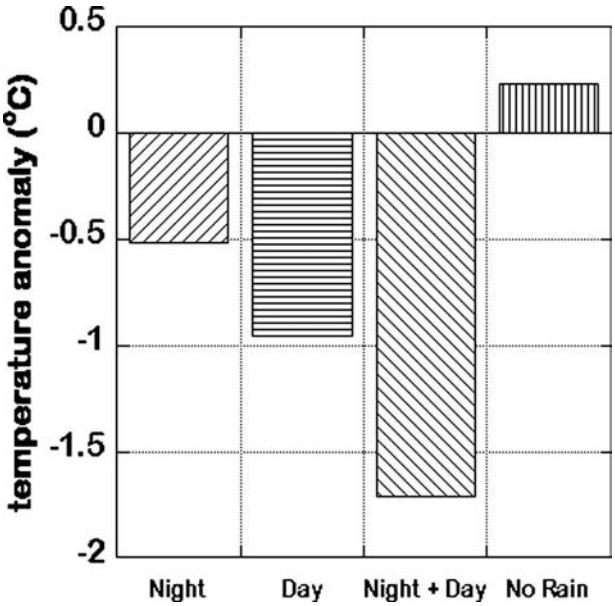

Fig. 3. The JJA 1977–2004 mean anomaly of the daily maximum temperature for events in each of the four categories: nighttime (1500–0400 LST) rain, daytime (0500–1400 LST) rain, nighttime and daytime rain, and no rain.

higher incident solar shortwave radiation and lower upward latent heat fluxes from the drier surfaces. Days following nights with rain were somewhat warmer than the other categories of rainy days because nighttime cloudiness reduces longwave radiation emission to space. Fewer daytime clouds also allow more solar input on the next day.

Table 1 gives the correlation coefficients between ΔT_y and each of seven other climate variables. While ΔT_y is positively correlated with the 500-mb geopotential height over the eastern United States, it is negatively correlated with eastern Pacific Ocean SSTA. (Considering Atlantic SSTA did not increase the amount of explained variance of ΔT_y.) We found that the 500-mb geopotential height over the eastern United States is negatively correlated with eastern Pacific Ocean SSTA. Thus, warm JJA surface air temperatures in the eastern United States coincide with midtropospheric ridging in the east and upstream troughing over anomalously cool eastern Pacific waters. Not only do large thicknesses between pressure surfaces in warm air elevate geopotential heights, but the consequent ridging also inhibits precipitation or reroutes precipitation-bearing systems, causing a synergistic impact that leads to even higher surface temperatures. Indeed, the JJA mean 500-mb geopotential height over the eastern United States was negatively correlated with both precipitation frequency during each summer and seasonal precipitation accumulations.

Table 1. Linear correlation coefficients between the seasonal mean maximum surface air temperature anomaly over the eastern United States vs the seasonal mean of the indicated variable during 1977–2004. All variables are computed for the same eastern U.S. area except the Pacific SSTA.

Independent variable	Correlation coefficient
Geopotential height, 500 mb	0.85**
Precipitation frequency	−0.68**
Pacific SSTA	−0.58**
Precipitation accumulation	−0.40*
u-component surface wind	0.25
v-component surface wind	0.22
Sea level pressure	0.11

* Statistically significant at the 99% confidence interval.
** Statistically significant at the 95% confidence interval.

Previously it was shown that no-rain days are warmer on the average than precipitation days. Table 1 also shows that the correlation between ΔT_y and precipitation frequency (the fraction of summer days with any precipitation) is highly significant (see also Fig. 4). Thus, seasons with more rainy days tend to be cooler. The correlation between ΔT_y and the regional average of accumulated summertime precipitation was less impressive, but still significant at the 95% confidence level. Taken together, these correlations can be explained as the effect of clouds inhibiting incident shortwave radiation and ground surface wetness increasing upward latent heat fluxes. The regional precipitation accumulation was not correlated with the total number of rain events, so rainfall did not necessarily occur more often in years with anomalously high accumulations. Moreover, no relationship was found between ΔT_y and the intensity of precipitation, suggesting that surface temperature is not sensitive to the summer-to-summer variability in the relative frequencies of convective versus nonconvective rain.

Table 2 shows multiple correlations between ΔT_y versus precipitation frequency, accumulated precipitation, and SSTA in the eastern Pacific. The combination of all three variables achieves a multiple correlation of 0.77, compared to $r = -0.68$ for ΔT_y against precipitation frequency alone. Removing precipitation accumulation as an independent variable lowers the explained variance of ΔT_y by very little, but removing SSTA has a slightly bigger impact. Aside from geopotential height, which is physically related to temperature, precipitation frequency is the most important of the variables tested for explaining the interannual variability of ΔT_y. This single variable accounts for some 46% of the variance of ΔT_y, and the linear combination of precipitation frequency with SSTA in the eastern Pacific accounts for an additional 11% of the variance.

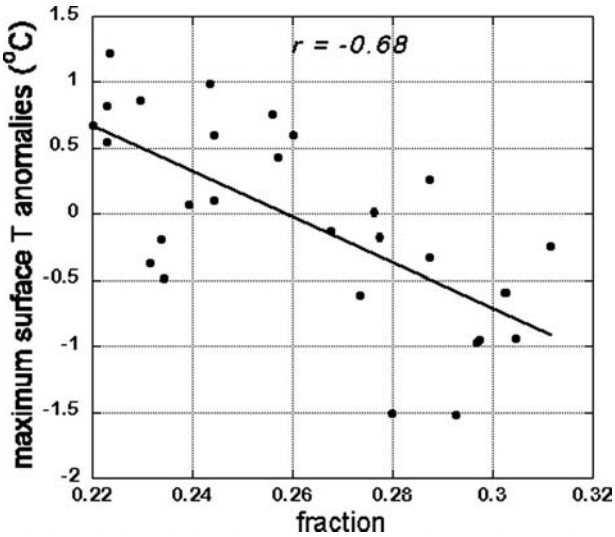

FIG. 4. Relationship between the JJA anomalies of mean maximum temperature for the eastern United States vs the fraction of rainy days in the corresponding seasons during 1977–2004.

Figure 5 shows the level of significance at each grid over the United States for correlations between the Pacific SSTA versus ΔT_y. Over most of the central and eastern United States, the maximum surface T at individual grid locations correlates with SSTA at a level of significance exceeding 95%.

b. *Evaluation of modeled precipitation characteristics*

These observational results are next compared to corresponding model results, using MM5 with the Betts–Miller, the Grell, or the Kain–Fritsch schemes. Figure 6 shows the partition of simulated events into the four categories (as defined above): precipitation only at night, only during the day, during both day and night, and no precipitation, for 24-h periods during JJA 1993–97. Compared to observational results (Fig. 2), all model versions overestimate the fraction of events with rain during night + day, but this error is especially large using the Grell scheme, which consequently underestimates the number of rain-free days. Simulations with the Betts–Miller and Kain–Fritsch schemes underestimate the no-rain fraction by a much smaller margin.

We next compare the timing of precipitation in MM5 simulations with observations in the southeastern United States, the focus of summertime afternoon rain showers. Figure 7a shows the diurnal variation of observed hourly rainfall for the combined summers, JJA 1993–97, averaged for stations within the area bounded by 30°–35°N, 92°–75°W. Figure 7b shows the same curves for the climate change experiments discussed below. The observed hourly precipitation reaches its peak value at 1700 LST, just after the time of maximum heating. Figure 7a shows that in MM5 simulations using the Grell scheme, accumulations increased steadily throughout the morning, peaking at about 1300 LST, some four hours too early, and the peak falls short of the observed value. The MM5 with Betts–Miller simulated somewhat more realistic amplitudes of diurnal precipitation maxima, but during the wrong part of the day, during the hours before 1000 LST. The Betts–Miller scheme's afternoon accumulations (between 1200 and 2000 LST) were considerably lower than observed. This diurnal cycle for the Betts–Miller scheme explains why surface temperatures in these simulations were so much higher than observed in the southeast United States (Lynn et al. 2004). The MM5 results using the Kain–Fritsch scheme achieve reasonable daytime amplitudes and peak only a little too early, although the morning hours are too rainy.

Figure 4 showed that observed JJA mean maximum surface temperature anomalies decrease as the fraction of rainy days increases. Figure 8a shows the frequency of rainy days per JJA season averaged for 1993–97 for each model and for station observations. Note that the spatial scale of the MM5 36-km grid is comparable to the distances between stations, but precipitation frequencies within AOGCM 4° × 5° grid elements are automatically greater because of the larger areas. Figure 8a therefore also shows a scaled frequency for groups of station observations within the AGCM's 4° × 5° grid elements. Even compared to the scaled observational frequency, precipitation is simulated much too often by the AOGCM, as well as by the Grell scheme.

TABLE 2. Multiple linear correlations between the seasonal mean maximum surface air temperature anomaly over the eastern United States vs the seasonal means of the indicated variables during 1977–2004. Variables are the same as in Table 1.

Independent variables	Correlation coefficient	Explained variance
Precipitation frequency, precipitation accumulation, SSTA	0.77	0.59
Precipitation frequency, SSTA	0.75	0.57
Precipitation frequency, precipitation accumulation	0.71	0.51
SSTA, precipitation accumulation	0.63	0.40

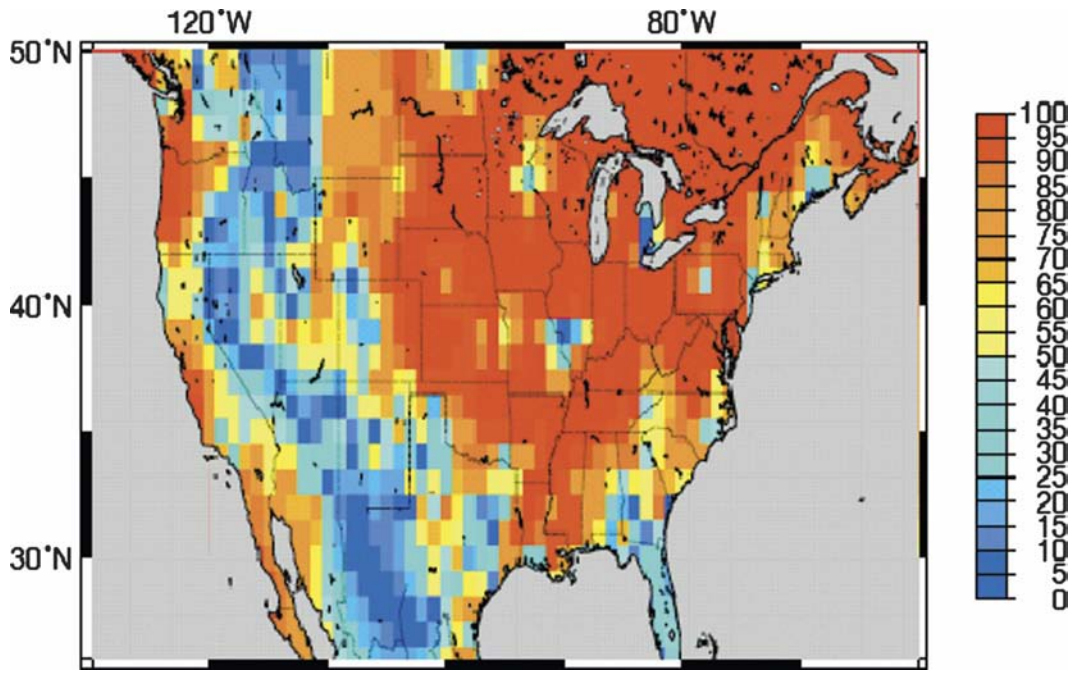

FIG. 5. Spatial distribution of the probability of statistical significance for correlations between JJA anomalies of the maximum surface air temperature interpolated from station observations vs normalized JJA Pacific sea surface temperature anomalies in the corresponding seasons during 1977–2004.

The simulated precipitation frequency for JJA 1993–97 is, however, only slightly too high for the Betts–Miller scheme. The precipitation frequency using the Kain–Fritsch scheme was too high, but it was lower than results with the AOGCM and the MM5 with the Grell scheme. Figure 8b shows that, despite high frequencies of precipitation, the AOGCM simulates less than half of the observed accumulation during JJA 1993–97. The seasonal accumulations for MM5 simulations with the Betts–Miller and Kain–Fritsch schemes were more realistic.

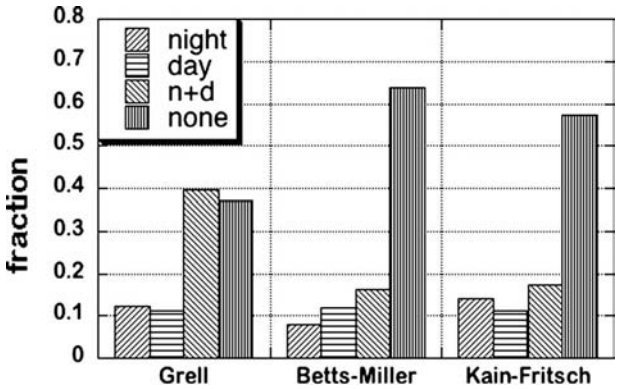

FIG. 6. The fractions of all simulated events during JJA 1993–97 for the four categories: nighttime rain (1500–0400 LST), daytime rain (0500–1400 LST), nighttime with daytime rain, and no rain, using the Betts–Miller scheme, the Grell scheme, and the Kain–Fritsch scheme.

Figure 9a shows the JJA 1993–97 mean surface temperature over the eastern United States for observations and for each model. The Betts–Miller scheme indicates the warmest conditions, no doubt a consequence of too little precipitation during the afternoon (Fig. 7a), while the Kain–Fritsch result matches observations. On the other hand, Fig. 9b indicates that the AOGCM and to a lesser extent the MM5 with the Grell scheme underestimate the daily maximum temperature compared to observations. This is consistent with their excessive frequency of precipitation (Fig. 8a) and the too early timing of the Grell daily precipitation maximum (Fig. 7a). Both models keep the ground surface wet too much of the time, so that excessive upward latent heat fluxes limit afternoon temperature maxima. The Betts–Miller solution is closest to the observed maximum temperature, while the Kain–Fritsch maximum exceeds the observed by 2.4°C. Reference to the results for the 1990s shown in Figs. 8a implies that modeling realistic temperature maxima may require simulation of a realistic frequency of precipitation events.

In summary, based on comparisons with 1993–97 observational evidence, the Kain–Fritsch moist convection scheme achieves the most realistic combination of mean temperature, precipitation diurnal cycle, and sea-

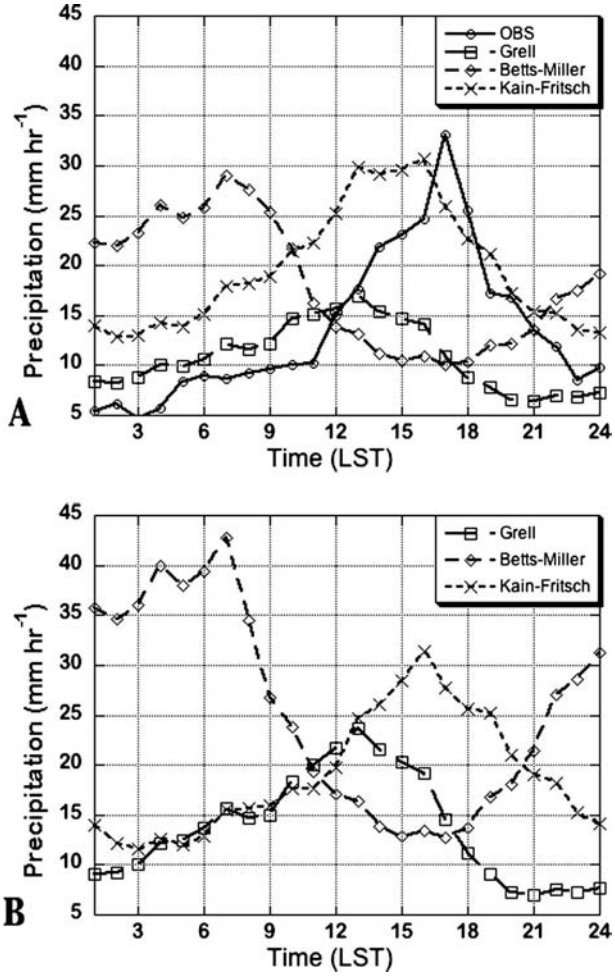

FIG. 7. The accumulated rainfall in the southeastern United States by hour for observations (○), simulations by the MM5 with the Grell scheme (□), with the Betts–Miller scheme (◊), and with the Kain–Fritsch scheme (×): (a) for the combined seasons, JJA 1993–97, and (b) for the combined seasons, JJA 2083–87.

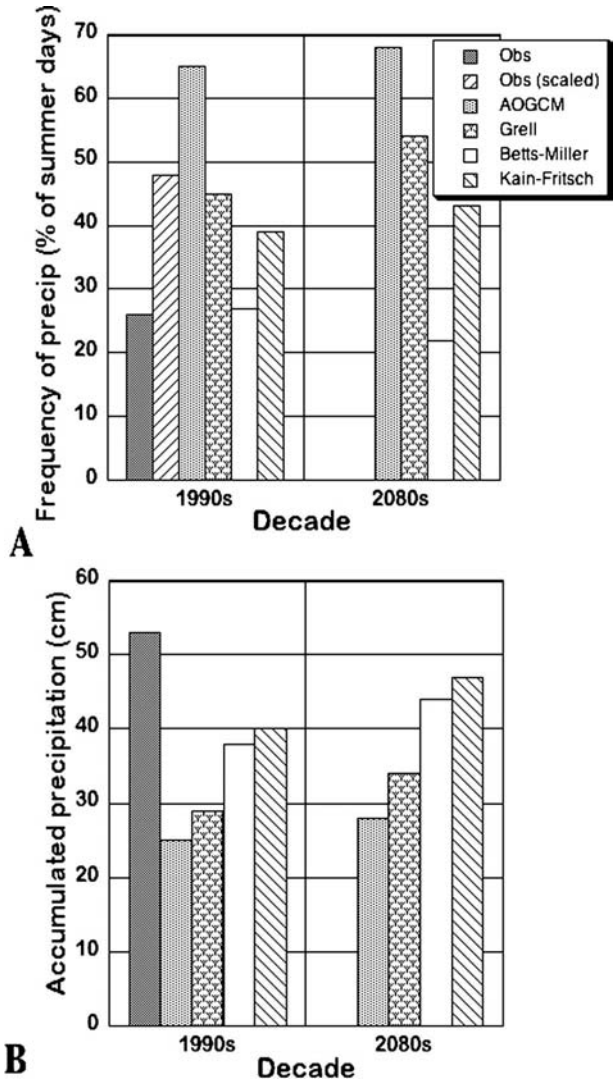

FIG. 8. Precipitation characteristics for JJA 1993–97 and JJA 2083–87 over the eastern United States for observations and model versions: (a) frequency: percent of rainy days during JJA, and (b) total JJA accumulations. "Scaled" observations refer to precipitation frequencies within 4° × 5° AOGCM grid elements.

sonal precipitation accumulation from among the three MM5 schemes. The Betts–Miller scheme achieves the most realistic precipitation frequency and maximum temperature but produces a very flawed diurnal cycle of precipitation.

c. *Climate change*

GISS AOGCM projected SSTA and atmospheric results according to the IPCC A2 climate change scenario were used to drive the MM5. The reliability of the data from the driving model affects the reliability of the nested model's simulations, even though downscaling to higher horizontal resolution improves the representation of climate fields. Validations of the AOGCM's performance over the entire Northern Hemisphere by Lucarini and Russell (2002) compared simulations of 1960–2000 trends in several climate variables, forced by observed increases in greenhouse gas concentrations, to corresponding NCEP reanalysis data. They found that the Northern Hemisphere spatial distributions of (AOGCM versus NCEP reanalysis) 40-yr trends in the annual mean surface air temperature (surface pressure) were correlated at $r = 0.52$ ($r = 0.49$), but trends of modeled JJA means were not correlated with the reanalysis. Trends in SST presumably parallel trends in the overlying surface air temperature, so these results are probably relevant for the AOGCM's SST simulations. Notwithstanding discrepancies in the validations,

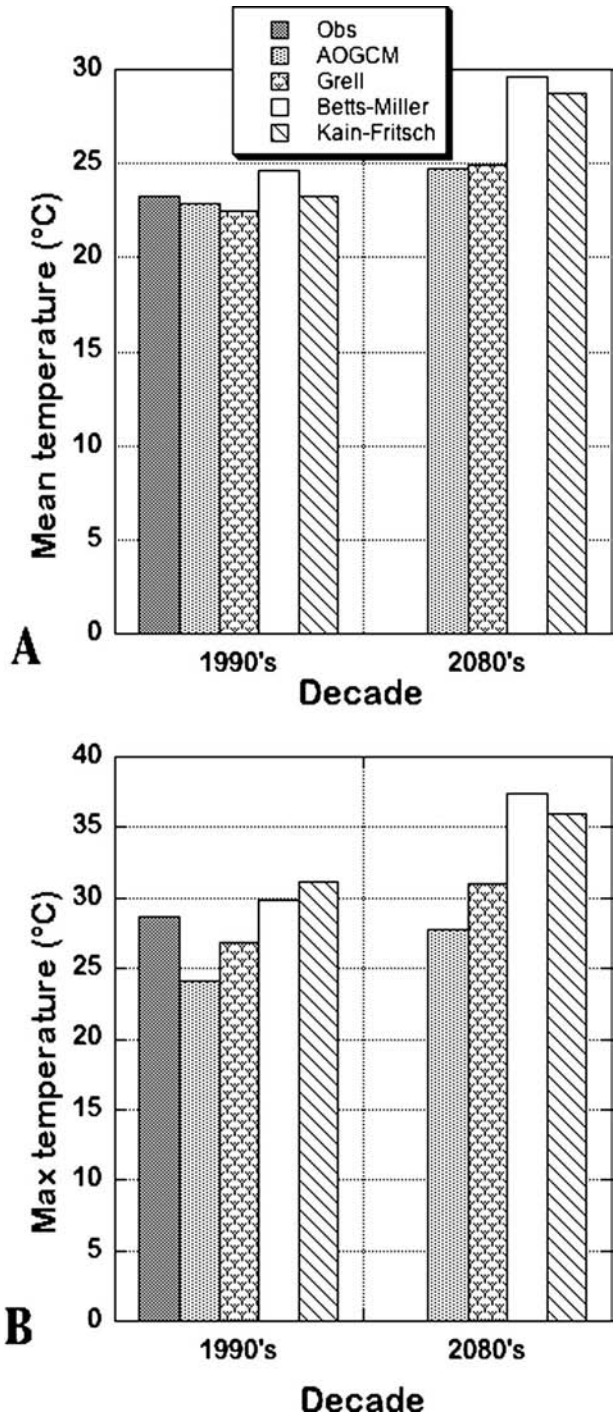

FIG. 9. Surface temperature characteristics for JJA 1993–97 and JJA 2083–87 over the eastern United States for observations and model versions: (a) means and (b) mean maximums.

Lucarini and Russell suggested that the AOGCM may be "reliable in forecasting future climate." Russell et al. (2000) showed spatial distributions of JJA 1960–98 trends in surface air temperature for the same AOGCM (their plate 2). The largest discrepancies between these modeled versus observed surface air temperature trends occur over the continents, where the model's simulations of summer rainfall are poor (G. Russell 2006, personal communication). Even so, the correspondence between model and observed trends appears quite good over the Pacific Ocean near the western boundary of the 108-km MM5 grid, where the AOGCM supplies information about planetary and Rossby waves entering the MM5 domain, while the trends are slightly less compatible over the Atlantic Ocean near the eastern boundary of the outer nested grid. Unrealistic features of the AOGCM simulation of some climate fields compromise the accuracy of the projections of climate change. However, mindful of the validations of its performance, the AOGCM's simulation of the IPCC A2 climate change scenario is as plausible as simulations from other IPCC models (G. Russell 2006, personal communication). Accordingly, the analysis of these downscaling experiments does provide valuable insight into the interpretation of regional climate change impacts.

The simulated frequency of precipitation and precipitation amounts for each model generally increased from the 1990s to the 2080s, although the precipitation frequency projected by the Betts–Miller scheme declined (Figs. 8a,b). Nevertheless, the relative magnitudes of frequencies and amounts among the models were ordered as in the 1990s. In the 2080s, the AOGCM and the Grell scheme continue to produce very high frequencies of precipitation. Moreover, Fig. 7b shows that the diurnal cycle of precipitation during the 2080s paralleled the outcome for the 1990s, whereby the Betts–Miller scheme consistently minimizes afternoon precipitation rates. Assuming the future diurnal cycle will resemble the observed in the 1990s, the Kain–Fritsch scheme remains the most realistic in this respect. Figure 9a indicates the mean temperature for the eastern United States for MM5 with the Betts–Miller, Grell, and Kain–Fritsch schemes and the GISS AOGCM simulations for JJA 2083–87. Figure 9b shows the corresponding JJA mean maximum surface temperature. The average surface temperatures of the 2080s were highest using Betts–Miller and lowest using Grell and the AOGCM. The high temperatures in the Betts–Miller results are consistent with unrealistically low afternoon precipitation. The relatively lower 2080s temperatures of the AOGCM and MM5 with the Grell scheme are undoubtedly influenced by unrealistically high frequencies of rainfall, as in the 1990s. An important consequence of the differences in modeled precipitation is that each model version shows a different sensitivity to climate change. Note that higher pro-

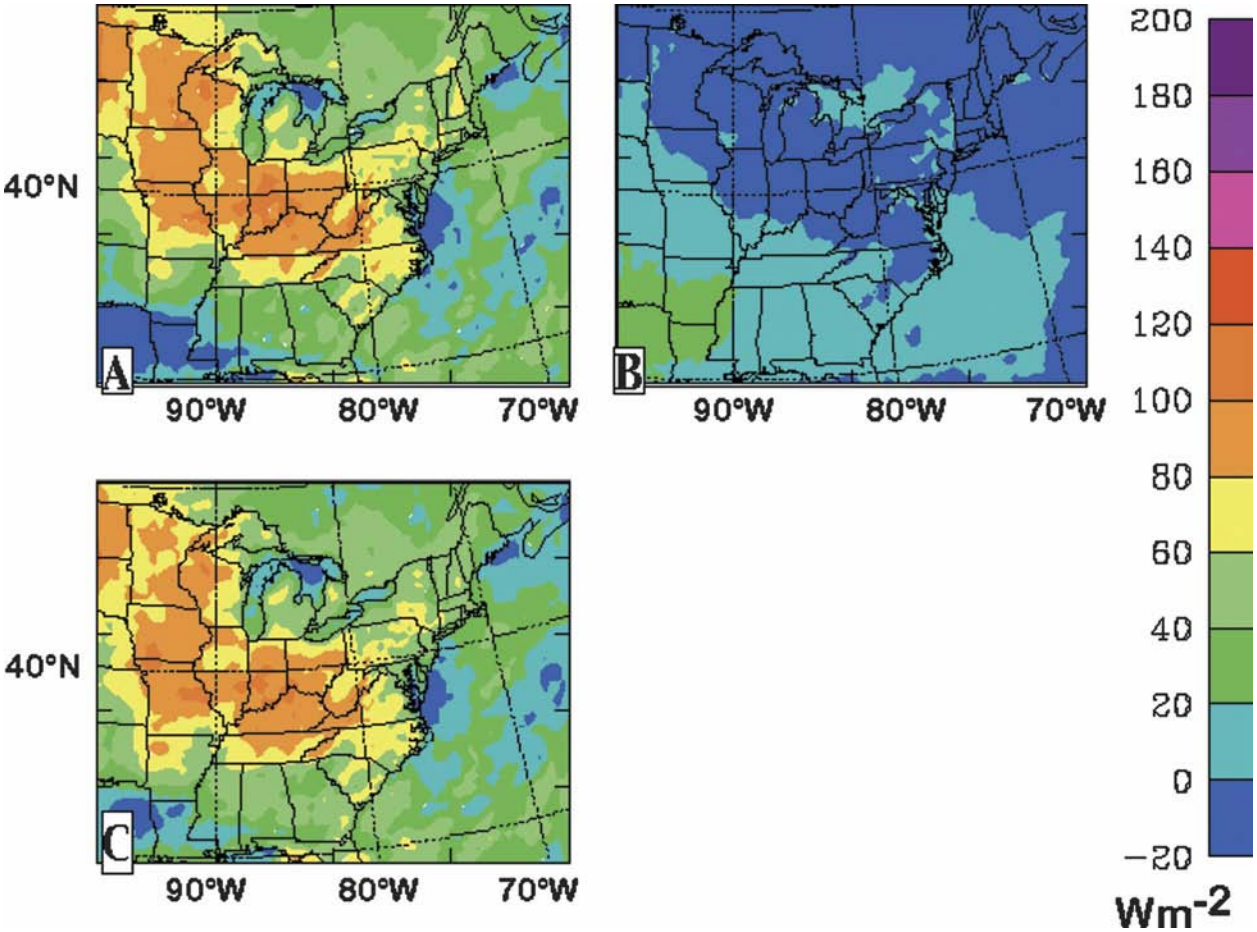

FIG. 10. Spatial distributions of simulation differences for July 1993 between two versions of the MM5, Kain–Fritsch minus Grell: (a) incident shortwave radiation flux at the earth's surface, (b) downward longwave radiation flux at the earth's surface, and (c) incident shortwave plus downward longwave radiation fluxes.

jected mean temperatures correspond to higher projected maximum temperatures. The Kain–Fritsch scheme's precipitation amount and mean temperature were realistic compared to 1990s observations, while its maximum temperature was 2.4°C too warm. The Betts–Miller scheme exhibited realistic precipitation frequency and maximum temperature in the 1990s. These versions' projections of a 5°–5.5°C mean temperature increase over the eastern United States are probably more credible than the AOGCM and Grell projections of only 1.8°–2.4°C. Note that the larger projected temperature changes are even large compared to the models' systematic temperature errors of only 0°–1.4°C for the 1990s (Fig. 9a).

Characteristics of the precipitation regime have dramatic effects on the surface radiation balance, which in turn affects surface air temperatures. This can be best illustrated by examining differences between MM5 simulations with contrasting outcomes using the Grell and Kain–Fritsch schemes and comparing them to the AOGCM results. The MM5 simulation using the Kain–Fritsch scheme was similar to the Betts–Miller simulation, except that it achieved a better diurnal cycle of precipitation (Fig. 7). We compare the spatial distributions of the surface radiation balance and the maximum surface air temperature simulated for July 1993 and July 2085, months that were both anomalously warm for their respective decades. In the July 1993 case shown in Fig. 10a, the Kain–Fritsch-based model experienced higher incident shortwave radiation than the simulation based on Grell, consistent with the generally lower simulated frequency of precipitation days by Kain–Fritsch (Fig. 8). Figure 10b shows rather small differences in longwave radiation at the ground surface between the two versions. The MM5 simulation using the Grell scheme features more frequent precipitation and consequently a lower Bowen ratio than the corresponding simulation based on the Kain–Fritsch scheme.

Differences in the combined downward fluxes, mostly reflecting the shortwave pattern (Fig. 10c), as well as a different partitioning between ground to air sensible and latent heat fluxes (not shown), explain the modest differences in MM5-simulated maximum surface temperatures in July 1993, shown in Fig. 11. AOGCM maximum surface air temperatures for July 1993 are consistently cooler than the results from both MM5 versions (Fig. 11c).

Figure 12 shows the corresponding shortwave and longwave flux difference fields for July 2085, the warmest month in the climate change experiment. Over the Midwest, positive differences in incident shortwave flux (Fig. 12a) are less than in July 1993, while across the southern states they are greater. However, an area of positive differences in downward longwave flux has expanded, and differences are larger over most of the region (Fig. 12b) compared with the earlier period (Fig. 10b). Thus, over most of the eastern United States, the Kain–Fritsch simulation experiences greater 2085 minus 1993 increases than Grell in the net downward radiation (shortwave plus longwave) at the ground surface (Fig. 12c), which is in part a consequence of higher downward longwave radiation flux associated with elevated concentrations of greenhouse gases. We found that vertical profiles of tropospheric temperature and specific humidity were higher in July 2085 for the Kain–Fritsch projection than the Grell. This suggests a possible feedback in the simulation based on Kain–Fritsch between warmer ground surface temperatures (over drier soils) and enhanced downward longwave radiation from warmer air with elevated concentrations of atmospheric water vapor. These differences in the surface radiation balance are consistent with the more pronounced warming in the Kain–Fritsch simulation compared to the Grell (Figs. 13a,b). Maximum temperatures for July 2085 simulated by the MM5 with the Kain–Fritsch scheme (Fig. 13b) are between 38° and 46°C across the southern states and about 38°C across 40°N. Notably, Pacific SSTA forcing for JJA 2085 was the coldest of all five seasons, consistent with the observed relationship discussed in section 3a. Moreover, the MM5 simulation using Kain–Fritsch simulated midtropospheric ridging over the Mississippi Valley in July 2085, while the simulation using the Grell scheme did not (not shown). Corresponding surface air temperatures with the Grell scheme (Fig. 13a) ranged from 30° to 38°C, while the AOGCM simulated maximum temperatures of only 26°–35°C (Fig. 13c).

Warming from increased concentrations of greenhouse gases involves a positive feedback characterized by positive trends of downward fluxes of longwave radiation. This downward longwave energy increased more in the climate change experiment using the Kain–Fritsch scheme, which simulated a realistic frequency and diurnal cycle of precipitation.

4. Summary and conclusions

The study concentrates on the variability of June–August (JJA) surface air temperatures over the eastern United States and the implications of this variability for decadal climate change. The analysis of the 28-yr (1977–2004) observational dataset showed that SSTAs in the eastern Pacific are well correlated with summertime surface air temperatures over broad areas of the eastern United States. An interaction between Pacific SSTA and atmospheric planetary waves was detected whereby cold SSTA are associated with midtropospheric ridging over the eastern United States. The ridging, in turn, coincides with positive temperature anomalies, promotes warm air advection into the eastern United States, and inhibits precipitation or reroutes precipitation-bearing systems, with a consequent positive feedback leading to even higher surface temperatures and a reinforcement of the ridging. Observations also showed that maximum surface temperatures in the eastern United States are higher on rainless days and coolest when it rains during the daylight hours until early afternoon. Moreover, the JJA mean maximum surface temperature anomaly is negatively correlated with the fraction of rainy days during each summer. The Pacific SSTA and the fraction of rainy days together account for about 57% of the interannual variance of the JJA maximum surface temperature anomaly in the eastern United States.

MM5 climate simulations on a nested 108-km outer–36-km inner grid were driven by atmospheric and SST boundary conditions simulated by the GISS AOGCM. Three alternative moist convection schemes for the MM5 produced simulation results for the 1990s with distinctly different precipitation characteristics. The AOGCM and the MM5 using the Grell scheme both generated an unrealistically high fraction of precipitation days, while the Betts–Miller scheme generally failed to produce afternoon peaks in convective rainfall. Mean JJA temperatures simulated by the Betts–Miller scheme were too high owing to the deficit of afternoon precipitation, and the JJA mean maximum temperature was too low in the AOGCM results and in the MM5 results using the Grell scheme, owing to their excessive frequency of rainy days. The diurnal cycle of precipitation using the Kain–Fritsch scheme was the most realistic, and its simulated fraction of rainy days was more realistic than with the Grell scheme, although still higher than observed. MM5 simulations for JJA

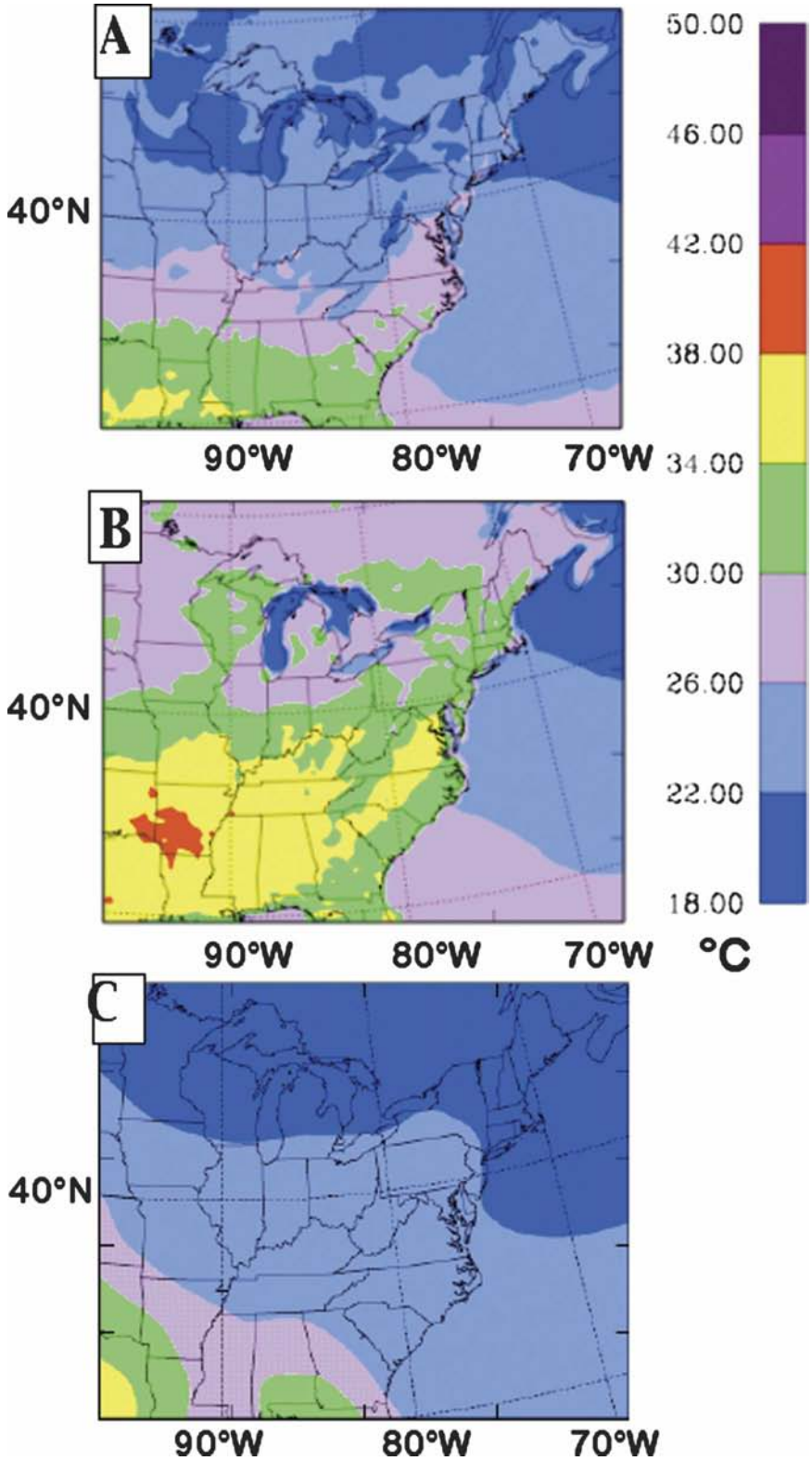

FIG. 11. Simulated maximum surface air temperatures for July 1993 from (a) the MM5 with the Grell moist convection scheme, (b) the MM5 with the Kain–Fritsch moist convection scheme, and (c) the AOGCM.

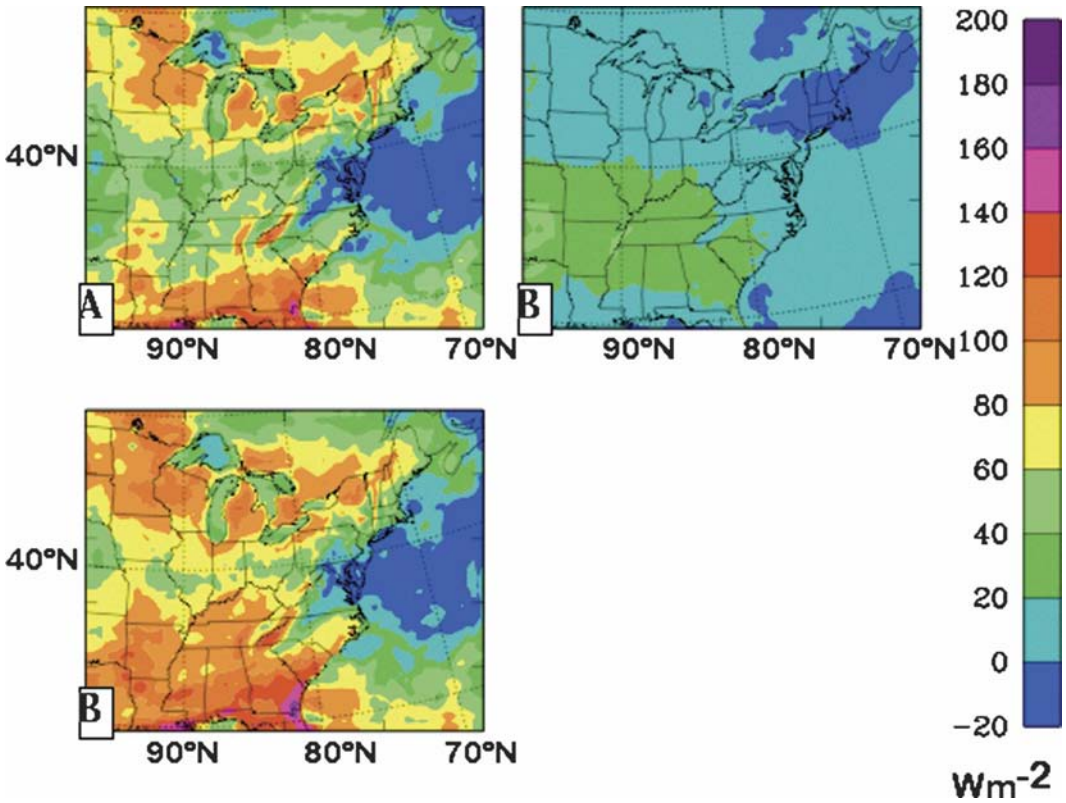

Fig. 12. Same as in Fig. 10, but for July 2085.

1993–97 with the Kain–Fritsch scheme also featured realistic mean surface air temperatures and the most realistic seasonal accumulations of precipitation from among the models that were tried.

AOGCM climate change projections according to the IPCC A2 scenario were downscaled to the 36-km grid by each of the three MM5 versions in time slice experiments corresponding to JJA during each of the years, 2083–87. While the accuracy of the AOGCM projections is disputable, they characterize a plausible representation of the future climate. Regional characteristics of this projected future climate based on each of the alternative MM5 downscaling approaches were compared and contrasted. Simulated precipitation frequencies, the diurnal timing of precipitation, and the diurnal temperature range in these MM5 simulations were quite similar to their corresponding characteristics in the 1990s simulations. For example, the AOGCM and the MM5 using the Grell scheme again featured unrealistically high frequencies of rainfall and concomitantly small diurnal temperature ranges, and they projected the lowest mean and the lowest maximum surface air temperatures for JJA 2083–87.

AOGCM SST projections provided considerable climate variability in the forcing for MM5 simulations during the 2080s. The very warm JJA 2085 season simulated by the MM5 with the Kain–Fritsch scheme was forced by a very negative SSTA in the eastern Pacific Ocean, paralleling the relationship documented from the 28-yr observational data. In contrast, a positive SSTA in the Pacific for JJA 2084 forced a rather cool summer in that simulation. During the warmest month, July 2085, the downscaling using the Kain–Fritsch parameterization projected monthly mean maximum temperatures of more than 38°C over large areas of the southeastern United States, even though the driving (AOGCM) simulation was projecting maximum temperatures below 35°C.

Analysis of the surface radiation budget detected important differences between the alternative simulations. One consequence of the frequent precipitation of the Grell scheme is that it inhibited the diurnal temperature range by high upward fluxes of latent heat and by the interception of incoming shortwave radiation by the associated cloudiness. In contrast, the model with the Kain–Fritsch scheme, which featured precipitation frequencies compatible with 1990s observations, a realistic JJA mean temperature, and realistic afternoon precipitation peaks, simulated larger increases in downward longwave radiation flux between July 1993 and

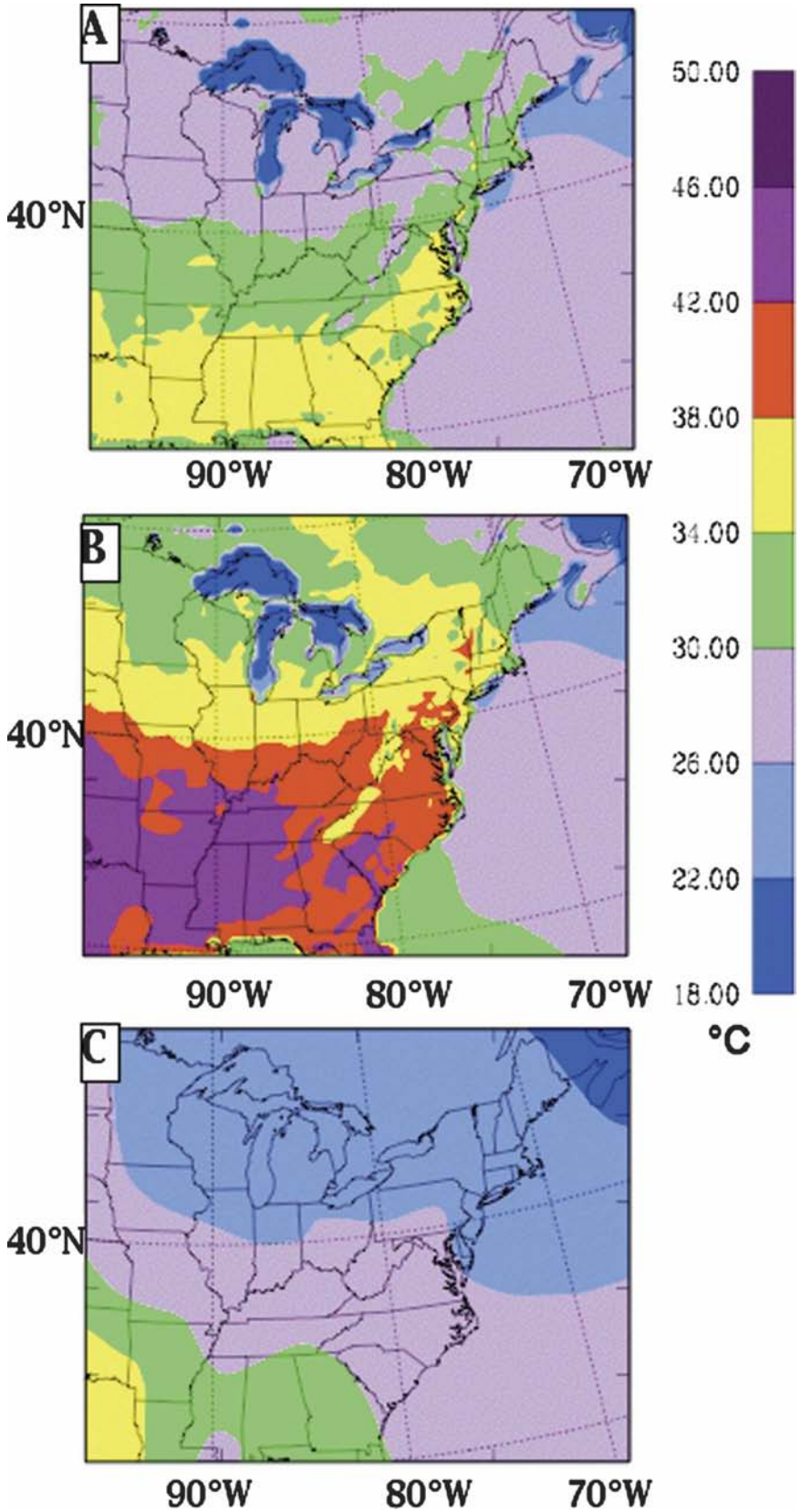

FIG. 13. Same as in Fig. 11, but for July 2085.

July 2085. These simulations projected an increase in the eastern U.S. JJA mean surface air temperature of 5.5°C between the 1990s and the 2080s. Thus, the most realistic simulation predicted a large increase in the mean temperature and mean maximum temperature, suggesting the potential for extreme temperature change.

Diffenbaugh et al. (2005) raise the possibility that negative anomalies of precipitation, soil moisture, clouds, and evapotranspiration during extreme hot events could interact in a mutually enhancing positive feedback with anomalous ridging aloft. They downscaled an IPCC A2 climate change scenario to a 25-km grid over the southwest United States with the Regional Climate Model version 3 (RegCM3) and found that geopotential heights and anticyclonic flow were both enhanced at 500 mb over the southwest United States and northern Mexico concomitant with the simulation of anomalously warm temperatures. Our results suggest that changes in the eastern U.S. geopotential height field were indeed involved in a positive feedback loop with changes in the surface energy balance related to simulated precipitation characteristics. This feedback over the eastern United States not withstanding, there is also strong evidence that eastern Pacific Ocean SSTA provides remote forcing that may initiate anomalous seasons over the eastern United States.

The current study shows that greenhouse warming effects were amplified in the simulations that included realistic precipitation frequencies, and they were damped in the simulations with exaggerated precipitation frequency. Results from the MM5 with the Grell scheme and from the GISS AOGCM demonstrate why projections of regional climate change by models that are prone to simulate rain too often (and at the wrong time of day) must be suspect. Atmospheric models with moist convection parameterizations that overestimate precipitation frequency may be challenged to predict extremely warm summers because they will fail to account for the important feedbacks between the surface energy balance, temperatures, and the large-scale circulation. We conclude that there is a potential for extreme temperature change that is not realized in many GCM simulations, but this potential can be detected by downscaling such GCM simulations with the appropriate mesoscale model.

Acknowledgments. This work was supported by the U.S. Environmental Protection Agency under Agreement RD-83096101-0, the NASA Climate and Earth Observing System Programs, and the CLIME Project of the New York City Department of Environmental Protection. BL was partially supported by NSF Grant ATM-0503152 and LD by NSF Grant ATM-0354589. We gratefully acknowledge the Data Support Section of the National Center for Atmospheric Research for providing meteorological observations and the NOAA Climate Diagnostics Center for providing reanalysis data used in the study. Thanks to Dr. Gary Russell for helpful discussions about the AOGCM.

REFERENCES

Bates, G. T., F. Giorgi, and S. W. Hostetler, 1993: Toward the simulation of the effects of the Great Lakes on regional climate. *Mon. Wea. Rev.,* **121,** 1373–1387.

Bell, J. L., L. C. Sloan, and M. A. Snyder, 2004: Regional changes in extreme climatic events: A future climate scenario. *J. Climate,* **17,** 81–87.

Betts, A. K., 1986: A new convective adjustment scheme. Part I: Observational and theoretical basis. *Quart. J. Roy. Meteor. Soc.,* **112,** 677–692.

——, and M. J. Miller, 1986: A new convective adjustment scheme. Part II: Single column tests using GATE wave, Bomex, ATEX and Artic air-mass data sets. *Quart. J. Roy. Meteor. Soc.,* **112,** 693–709.

Bunkers, M. J., J. R. Miller Jr., and A. T. Degaetano, 1996: An examination of El Niño–La Niña-related precipitation and temperature anomalies across the Northern Plains. *J. Climate,* **9,** 147–160.

Chen, F., and J. Dudhia, 2001a: Coupling an advanced land surface–hydrology model with the Penn State–NCAR MM5 modeling system. Part I: Model implementation and sensitivity. *Mon. Wea. Rev.,* **129,** 569–585.

——, and ——, 2001b: Coupling an advanced land surface–hydrology model with the Penn State–NCAR MM5 modeling system. Part II: Preliminary model validation. *Mon. Wea. Rev.,* **129,** 587–604.

Diffenbaugh, N. S., J. S. Pal, R. J. Trapp, and F. Giorgi, 2005: Fine-scale processes regulate the response of extreme events to global climate change. *Proc. Natl. Acad. Sci. USA,* **102,** 15 774–15 778.

Dudhia, J., 1993: A nonhydrostatic version of the Penn State–NCAR Mesoscale Model: Validation tests and simulation of an Atlantic cyclone and cold front. *Mon. Wea. Rev.,* **121,** 1493–1513.

Giorgi, F., G. Bates, and S. Nieman, 1993: The multiyear surface climatology of a regional atmospheric model over the western United States. *J. Climate,* **6,** 75–95.

Grell, G., 1993: Prognostic evaluation of assumptions used by cumulus parameterizations. *Mon. Wea. Rev.,* **121,** 764–787.

——, Y.-H. Kuo, and R. J. Pasch, 1991: Semiprognostic tests of cumulus parameterization schemes in the middle latitudes. *Mon. Wea. Rev.,* **119,** 5–31.

——, J. Dudhia, and D. R. Stauffer, 1994: A description of the fifth-generation Penn State/NCAR mesoscale model (MM5). NCAR Tech. Note NCAR/TN-298+STR, 117 pp.

Han, J., and J. Roads, 2004: US climate sensitivity simulated with the NCEP Regional Spectral Model. *Climatic Change,* **62,** 115–154.

Hansen, J., G. Russell, D. Rind, P. Stone, A. Lacis, S. Lebedeff, R. Ruedy, and L. Travis, 1983: Efficient three-dimensional global models for climate studies: Models I and II. *Mon. Wea. Rev.,* **111,** 609–662.

Hogrefe, C., and Coauthors, 2004: Simulating regional-scale

ozone climatology over the eastern United States: Model evaluation results. *Atmos. Environ.,* 38, 2627–2638.

Hu, Q., and S. Feng, 2002: Interannual rainfall variations in the North American summer monsoon region: 1900–98. *J. Climate,* **15,** 1189–1202.

Janjic, Z., 1994: The step-mountain eta coordinate model: Further development of the convection, viscous sublayer, and turbulent closure schemes. *Mon. Wea. Rev.,* **122,** 927–945.

Kain, J. S., and J. M. Fritsch, 1993: Convective parameterization for mesoscale models: The Kain-Fritsch scheme. *The Representation of Cumulus Convection in Numerical Models, Meteor. Monogr.,* No. 46, Amer. Meteor. Soc., 165–170.

Knowlton, K., and Coauthors, 2004: Assessing ozone-related health impacts under a changing climate. *Environ. Health Perspect.,* **112,** 1557–1563.

Kushnir, Y., 1994: Interdecadal variations in North Atlantic sea surface temperature and associated atmospheric conditions. *J. Climate,* **7,** 141–157.

——, and N.-C. Lau, 1992: The general circulation model response to a North Pacific SST anomaly: Dependence on time scale and pattern polarity. *J. Climate,* **5,** 271–283.

Lau, N.-C., 1997: Interactions between global SST anomalies and the midlatitude atmospheric circulation. *Bull. Amer. Meteor. Soc.,* **78,** 21–33.

Leung, L. R., Y. Qian, and X. Bian, 2003a: Hydroclimate of the western United States based on observations and regional climate simulation of 1981–2000. Part I: Seasonal statistics. *J. Climate,* **16,** 1892–1911.

——, ——, ——, and A. Hunt, 2003b: Hydroclimate of the western United States based on observations and regional climate simulation of 1981–2000. Part II: Mesoscale ENSO anomalies. *J. Climate,* **16,** 1912–1928.

——, ——, ——, W. M. Washington, J. Han, and J. D. Roads, 2004: Mid-century ensemble regional climate change scenarios for the western United States. *Climatic Change,* **62,** 75–113.

Liang, X.-Z., L. Li, and K. E. Kunkel, 2004: Regional climate model simulations of U.S. precipitation during 1982–2002. Part I: Annual cycle. *J. Climate,* **17,** 3510–3529.

Lucarini, V., and G. Russell, 2002: Comparison of mean climate trends in the Northern Hemisphere between National Centers for Environmental Prediction and two atmosphere-ocean model forced runs. *J. Geophys. Res.,* **107,** 4269, doi:10.1029/2001JD001247.

Lynn, B. H., and Coauthors, 2004: Sensitivity of present and future surface temperatures to precipitation characteristics. *Climate Res.,* **28,** 53–65.

Mearns, L. O., R. W. Katz, and S. H. Schneider, 1984: Extreme high-temperature events: Changes in their probabilities. *J. Climate Appl. Meteor.,* **23,** 1601–1613.

Meehl, G. A., F. Zwiers, J. Evans, T. Knutson, L. Meams, and P. Whetton, 2000: Trends in extreme weather and climate events: Issues related to modeling extremes in projections of future climate change. *Bull. Amer. Meteor. Soc.,* **81,** 427–436.

Nobre, P., A. D. Moura, and L. Sun, 2001: Dynamical downscaling of seasonal climate prediction over Nordeste Brazil with ECHAM3 and NCEP's Regional Spectral Models at IRI. *Bull. Amer. Meteor. Soc.,* **82,** 2787–2796.

Russell, G. L., J. R. Miller, and D. Rind, 1995: A coupled atmosphere–ocean model for transient climate change studies. *Atmos.–Oceans,* **33,** 683–730.

——, ——, ——, R. Ruedy, G. Schmidt, and S. Sheth, 2000: Comparison of model and observed regional temperature changes during the past 40 years. *J. Geophys. Res.,* **105** (D11), 14 891–14 898.

Straus, D. M., and F. Molteni, 2004: Circulation regimes and SST forcing: Results from large GCM ensembles. *J. Climate,* **17,** 1641–1656.

Ting, M., and H. Wang, 1997: Summertime U.S. precipitation variability and its relation to pacific sea surface temperature. *J. Climate,* **10,** 1853–1873.

Trenberth, K. E., A. Dai, R. Rasmussen, and D. Parsons, 2003: The changing character of precipitation. *Bull. Amer. Meteor. Soc.,* **84,** 1205–1217.

Walsh, K., and J. L. McGregor, 1995: January and July climate simulations over the Australian region using a limited-area model. *J. Climate,* **8,** 2387–2403.

Ye, H., 2001: Characteristics of winter precipitation variation over northern central Eurasia and their connections to sea surface temperatures over the Atlantic and Pacific Oceans. *J. Climate,* **14,** 3140–3155.